JOURNAL OF COMPUTATIONAL PHYSICS **20**, 1–21 (1976)

A Numerical Investigation into the Solution of the Equations Describing Baroclinic–Barotropic Instability in the Atmosphere

IAN DAVID KANE

Department of Meteorology, Imperial College, London

Received September 11, 1974; revised May 19, 1975

A numerical solution to the equations for small linearized perturbations of a mean zonal flow containing both lateral and vertical shear is investigated using three time difference schemes, two of which are discarded. The chosen scheme is weakly unstable. The time step has a lower bound as well as the C.F.L. condition upper bound; for fixed time step and allowable growth rate error, there is an upper bound to the vertical resolution for fixed computing time. Total integration time to convergence is speeded up by a good choice of initial field and problems of degenerate eigenvalues are overcome by a variation of the method whereby only the dominant wave remains. To obtain a complete spectrum of eigenvalues, the direct Q.R. method of solution proved far more efficient than time integration.

1. INTRODUCTION

The global scale transfer of energy and momentum in the earth's atmosphere is brought about mainly by quasi-geostrophic (baroclinic) eddies. The mean flow, upon which these eddies are superimposed, is determined by the latitudinal variations of temperature (imposed by global-scale variations in net heating) that force slow axially-symmetrical adjustments, during which angular momentum is conserved and thermal–wind balance for the zonal flow is established. The energy transfer due to this meridional circulation is generally small, and the conversion of latent into sensible energy and the creation of thermal–wind balance are its most important properties. More detailed discussion can be found in [4, 8, 10], but the general inference is that the intensity and structure of the zonal circulation is determined by the horizontal gradient of temperature. This gradient is in turn determined by the temperature contrast that the baroclinic eddies need in order to relax the radiatively determined energy imbalance by large-scale horizontal heat transport.

The generation of the eddies can be studied as the amplification of small amplitude perturbations on a given mean zonal flow, during which phase the characteristic scale and structure of the eddies is determined. Such definition of

structure is of fundamental importance for the parametric representation of the eddy transfer (their momentum transfer being particularly subtle). The object of this work was to determine the structure of the perturbation solutions for fairly realistic zonal mean winds in order to supplement the information gained from classical studies [2, 3, 7] that treat only highly idealized states.

There is, however, a second field of application, for the problem of numerical weather prediction is largely concerned with calculating the growth, speed, and scale of newly developing large-scale systems within which the samller-scale processes of weather (such as frontal zones) develop. Clearly the viable representation of the perturbation solutions is a necessary, though not sufficient, criterion for such prediction schemes, and the general impression is that only those schemes with extremely high resolution come anywhere near representing the analytically defined fluid dynamics in this respect.

This then is the aim of the study: to determine the structure of the growing waves and to comment on the effects of truncation in finite-difference representations. The second of these aims will be treated here, the first reported on in a meteorological context.

The motion is assumed to be adiabatic, the horizontal flow is assumed nearly geostrophic, and the variation of Coriolis parameter with latitude is taken into account only where it is differentiated. Consistently, a tangent-plane approximation to the earth's spherical geometry is used, with rigid walls at the equator and at the polar limit of the system that correspond to a latitude of about 60° on the earth (the "quasi-geostrophic beta-plane" approximation). A rigid lid replaces the tropopause and the variation of mean density with height is neglected (the effect of these on amplifying waves being fairly well known [7]). The initial zonal velocity is in general a function of both height and latitude, in which respect the study represents a generalization of the classical studies in which the zonal velocity is supposed a function of height only.

2. Basic Equations

Scale analysis shows that if the relative accelerations are much smaller than the Coriolis accelerations (small Rossby number), then the motion satisfies the quasi-geostrophic vorticity equation [7]

$$\frac{\mathrm{D}\zeta}{\mathrm{D}t_h} + v\beta = f\frac{\partial}{\partial z}(w) \tag{1}$$

with $\mathrm{D}/\mathrm{D}t_h$ = differentiation following horizontal motion; ζ = vertical component of relative vorticity; v = south→north velocity; $\beta = \partial f/\partial y$, variation of

Coriolis parameter with latitude; z = height above sea level (*strictly* geopotential height); and w = vertical velocity.

To the same order of approximation, the continuity equation is

$$\frac{\partial u}{\partial x} + \frac{\partial v}{\partial y} = 0 \tag{2}$$

with u = west→east velocity. This implies a streamfunction Ψ with $u = -\partial\Psi/\partial y$, $v = \partial\Psi/\partial x$, and $\zeta = \Psi_{xx} + \Psi_{yy}$.

Small perturbations are made from an initial state where pressure, density, and entropy are functions of height and latitude only and where the initial flow is zonal $U_0(y, z)$.

With the thermodynamic equation for dry adiabatic motion

$$\frac{D\Phi}{Dt_h} + w\frac{\partial\Phi}{\partial z} = 0, \tag{3}$$

where Φ is the log potential temperature, and for perturbations, $\phi(x, y, z)$ of entropy and $\psi(x, y, z, t)$ of streamfunction. Hydrostatic and thermal-wind balance for the perturbed flow demands that the vertical variation of velocity and the temperature be connected:

$$\phi = \frac{f}{g}\frac{\partial\psi}{\partial z}$$

and the equations reduce to the linearized form

$$\left(\frac{\partial}{\partial t} + U_0\frac{\partial}{\partial x}\right)\left(\psi_{xx} + \psi_{yy} + \frac{f^2}{gB}\psi_{zz}\right) + \frac{\partial\psi}{\partial x}\left(\beta - \frac{\partial^2 U_0}{\partial y^2} - \frac{f^2}{gB}\frac{\partial^2 U_0}{\partial z^2}\right) = 0 \tag{4}$$

where $B = \partial\Phi_0/\partial z$, the static stability. Eq. (4) is to be solved in a region

$$-\frac{L}{2} \leqslant y \leqslant \frac{L}{2}, \qquad 0 \leqslant z \leqslant H$$

with L = representatitive distance between pole and equator, taking account of the diminished area of the polar cap; and H = depth of the troposphere.

Rigid walls are taken as boundaries at pole, equator, surface, and tropopause, implying ψ = constant (taken as zero) at $y = \pm L/2$ and,

$$\left(\frac{\partial}{\partial t} + U_0\frac{\partial}{\partial x}\right)\frac{\partial\psi}{\partial z} - \frac{\partial U_0}{\partial z}\frac{\partial\psi}{\partial x} = 0 \qquad \text{at} \quad z = 0, H \tag{5}$$

from Eq. (3).

Equations (4) and (5) are the basic equations and boundary conditions to which solutions are sought. With $\psi(x, y, z, t) = G(y, z) \exp i\lambda(x - \bar{c}t)$, they define an eigenvalue problem for a given zonal wavelength $2\pi/\lambda$, with eigenvalue $\bar{c}$. In general, $\bar{c}$ is complex and then $\bar{c} = \bar{c}_r + i\bar{c}_i$, $\psi = G \exp \lambda\bar{c}_i t \exp i\lambda(x - \bar{c}_r t)$, where $\bar{c}_r$ represents a phase speed and $\lambda\bar{c}_i$ the growth rate.

3. Form of the Eigenvalue Spectrum

Solutions in general can be found only by numerical methods since, with $U_0(y, z)$, solutions are not generally separable. The equations are nondimensionalized to

$$\begin{aligned} (A(y)z - c)(NG_{yy} + G_{zz} - \nu^2 G) + G(\gamma - NzA_{yy}) &= 0 \\ (A(y)z - c)(\partial G/\partial z) - A(y)G &= 0 \qquad \text{at} \quad z = 0, 1 \\ G &= 0 \qquad \text{at} \quad y = \pm 1 \end{aligned} \tag{6}$$

with $y \to (2y/L)$, $z \to (z/H)$; $U_0(y, z) = \alpha_1 HA(y)z$ (where we have put U_0 linear with height), and $c = \bar{c}/(\alpha_1 H)$, $(c = c_r + ic_i)$; where $\nu^2 = \lambda^2 gB/f^2$, the square of the horizontal wavenumber; $\gamma = gBH\beta/(\alpha_1 f^2)$, generalized β-parameter; and $N = 4gBH^2/(f^2L^2)$.

The parameter α_1 is the vertical wind shear at $y = 0$, so that $A(y)$ is normalized to 1 at $y = 0$. The ratio of vertical to horizontal scales of the flow is represented by $N^{1/2}$.

To get an impression of the form of the complete eigenvalue spectrum for general values of U_0, the special case is taken with $A(y) \equiv 1$, i.e., baroclinic flow with $U_y = 0$ and constant shear. The set (6) then reduces to the one-dimensional problem whose solution is known from [7].

$$\begin{aligned} (z - c)\left(f_{zz} - \left(\nu^2 + N\frac{n^2\pi^2}{4}\right)f\right) + \gamma f &= 0 \\ (z - c)f_z - f &= 0 \qquad \text{at} \quad z = 0, 1 \end{aligned} \tag{7}$$

where $G(y, z) = f_n(z) \sin n\pi((1 - y)/2)$.

Figures 1 and 2 show the growth rates and phase speeds of the first seven modes, using data from Green's model with $\gamma = 1$.

Growing waves exist for all wavelengths, with the fastest growing wave for $n = 1$ but changing to other modes for longer and shorter waves; the growth rates of all modes are similar.

Solutions to (6) are now sought for general profiles of U by numerical methods. In particular, methods of obtaining the fastest growing wave for different wavelengths are examined and compared, as, according to the hypothesis of development

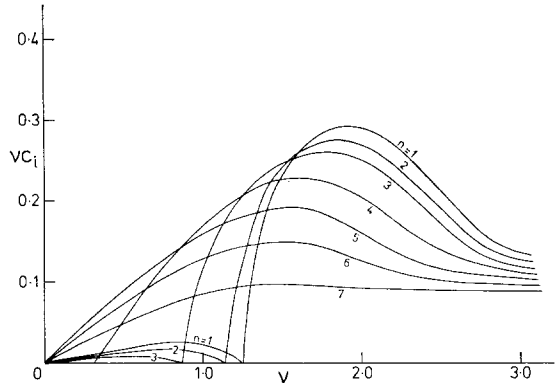

FIG. 1. Growth rate (νc_i) against wavenumber (ν) for flow $U = z$, mode $= n$, $L = 10{,}000$ km.

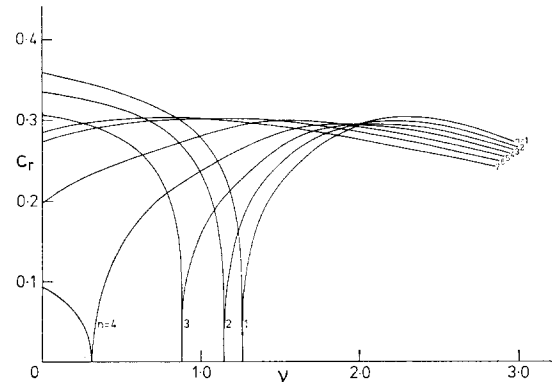

FIG. 2. Phase speed (c_r) against wavenumber (ν) for flow $U = z$, mode $= n$, $L = 10{,}000$ km.

from some initial infinitesimal arbitrary disturbance, these are the ones that will eventually dominate the motion. The numerical solution is of special interest because all of its difficulties also occur in the numerical prediction of quasi-geostrophic motion (although there are more numerical problems in (NWP), but the errors incurred can be analyzed fully here.

4. Integration Forward in Time

By analogy with the weather-prediction problem the linearized wave equation can be integrated forward in time and eventually the fastest growing mode will dominate.

With the transformation $t \to \lambda\alpha_1 Ht$, (or new t equivalent to about $t/4$ days), (4) and (5) transform (with $\psi = F(y, z, t) \exp i\lambda x$) to

$$\left[\frac{\partial}{\partial t} + i(MU_s + Az)\right](NF_{yy} + F_{zz} - \nu^2 F) + iF(\gamma - NzA_{yy} - NMU_{0_{yy}}) = 0$$

$$\left[\frac{\partial}{\partial t} + i(MU_s + Az)\right]\frac{\partial F}{\partial z} - iAF = 0 \qquad \text{at} \quad z = 0, 1 \tag{8}$$

$$F = 0 \qquad y = \pm 1.$$

The method of solution is one of time integration from an initial field $F(y, z, t = 0)$. We can suppose that F contains terms like $F_\nu(y, z, t) = \sum_j A_j a_j \exp -ic_j t$, where a_j are the normalized eigenfunctions, c_j are the corresponding eigenvalues, and A_j are the coefficients (found from the initial value of F). Eventually, F will grow steadily with a growth rate corresponding to the eigenvalue with largest imaginary part. Therefore, with finite-difference replacements to (8) and a given value for ν, the time integration is performed and terminated when values of F at all gridpoints grow at a steady growth rate (the method used in [1]). This method of solution is sometimes known as the power method [6]. Here various time difference schemes are analyzed for the replacement of $\partial F/\partial t$, but spatial centered differences replace spatial derivatives. The coordinate y, z is specified by the replacement

$$y \to k\,\Delta y - 1 \qquad z \to (l - 1)\,\Delta z$$

where Δy, Δz are horizontal and vertical gridlength, and k, l are the kth and lth gridpoints.

The variable A is chosen to be symmetric about $y = 0$, so that the solutions are either symmetric or antisymmetric, the former with $\partial F/\partial y = 0$ at $y = 0$ and the latter with $F = 0$ at $y = 0$, and the horizontal dimension can be halved.

The range of y, z in (8) is now

$-1 < y < 0$	even modes
$-1 < y \leqslant 0$	odd modes
$-\Delta z \leqslant z \leqslant 1 + \Delta z$	as $\partial F/\partial z$ appears in the boundary conditions.

The stability of the time integration is now analyzed for different schemes, and their stability examined. It is found that some stable schemes involve too much computer time to be of practical use and a scheme that is weakly unstable is chosen. The approach is to Fourier analyze in space the error in the solution of the finite-difference replacement of (8). For the purpose of this calculation, where advection is of major importance, the flow is taken to be constant (independent of y and z).

At time $t = \tau\,\Delta t$, let $E(y, z, t) = E_\tau$ be the error in F.

(a) *Forward Differences*

With $\partial F/\partial t$ replaced by $(F(t + \Delta t) - F(t))/\Delta t$, and with

$$E_\tau = \sum_{m,n} V_\tau(m, n) \exp i(mk\,\Delta y + nl\,\Delta z),$$

(8) implies

$$E_\tau = \sum_{m,n} V_0(1 + \kappa^2)^{\tau/2} \exp i(mk\,\Delta y + nl\,\Delta z + \tau \tan^{-1} \kappa) \tag{9}$$

with

$$\kappa = \frac{\gamma\,\Delta t}{(\bar{\kappa} + \nu^2)}, \qquad \bar{\kappa} = \frac{4N}{\Delta y^2} \sin^2 \frac{m\,\Delta y}{2} + \frac{4}{\Delta z^2} \sin^2 \frac{n\,\Delta z}{2}$$

and approximate κ to Δt. (γ is of the same order as $\bar{\kappa} + \nu^2$.)

The error grows exponentially and generates error E_c in c given by

$$\exp E_c t = \exp(\tau/2) \log(1 + \Delta t^2) = \exp(t\,\Delta t/2) \qquad \text{for small } \Delta t, \tag{9a}$$

implying $E_c \sim (\Delta t/2)$.

Assuming the growth rates for general mean flows are of the same order as those shown in Fig. 1, i.e., $\sim$0.2, and the maximum allowable error in the numerical value of the growth rate is $\sim \pm 0.005$ (for $\nu \sim 1$), denoted by E_c, (9a) implies $\Delta t \sim < 0.02$.

(b) *Euler Backward*

Again we have $\partial F/\partial t$ replaced by $(F(t + \Delta t) - F(t))/\Delta t$, but now the integration is repeated using the same replacement as above for terms involving $\partial F/\partial t$, but using computed values of $F(t + \Delta t)$ for terms *not* involving $\partial F/\partial t$. This implies a scheme

$$F^* = F(t) + \Delta t \left.\frac{\partial F}{\partial t}\right|_t$$

$$F(t + \Delta t) = F(t) + \Delta t \left.\frac{\partial F}{\partial t}\right|_*$$

and then (9) is replaced with

$$E_\tau = \sum_{m,n} V_0(1 + \kappa^4 - \kappa^2)^{\tau/2} \exp i \left(mk\,\Delta y + nl\,\Delta z - \tau \tan^{-1} \frac{\kappa}{1 - \kappa^2}\right)$$

which is numerically stable if $|\kappa| \leqslant 1$ and all the error is concentrated in the real part of the phase speed. This is the C.F.L. condition: $\Delta t \leqslant 1/|U - c_r|$, where c_r = nondimensional Rossby wave speed (Brown [1]).

(c) *Double and Single Difference Scheme* [11]

Although scheme (b) is stable, the repeated integration needed to advance one time step uses a large amount of computer time. To reduce this, a scheme is considered whereby the even time steps are advanced by method (b) and the odd time steps by method (a). This implies

$$E_{2\tau} = \sum_{m,n} V_0(1 + \kappa^6)^{\tau/2} \exp i\left(mk\,\Delta y + nl\,\Delta z + \tau \tan^{-1}\frac{2\kappa - \kappa^3}{1 - 2\kappa^3}\right) \qquad (10)$$

and the error in c_i is given by $E_c \sim (\Delta t)^5/4$. Therefore, with $E_c \sim \pm 0.005$, $\Delta t \sim <\frac{1}{2}$.

This method, although weakly unstable, reduces the integration time by a factor of 4 and is used in the following calculations. It is referred to subsequently as the DS scheme.

(d) *Centered Differences*

With $\partial F/\partial t$ replaced by $(F(t + \Delta t) - F(t - \Delta t))/2\Delta t$, as is commonly used in numerical prediction, and with $E_\tau = \sum V_\tau(m, n) \exp i(mk\,\Delta y + nl\,\Delta z)$, (8) gives $V_{\tau+1} = V_{\tau-1} + 2i\kappa V_\tau$ and then

$$E_\tau = \sum_{m,n} V_0 \exp i\left(mk\,\Delta y + nl\,\Delta z + \tau \tan^{-1}\frac{\kappa}{(1 - \kappa^2)}\right)$$

$$+ V_1 \exp i\left(mk\,\Delta y + nl\,\Delta y - \tau \tan^{-1}\frac{\kappa}{(1 - \kappa^2)}\right).$$

If $\kappa < 1$, the scheme is stable and the only error will be that found in the initial state. However, as the wave we are examining is growing, its amplitude will eventually become greater that V_0, V_1, and this error will be negligible.

5. Temporal and Spatial Truncation Errors

(a) *Temporal Truncation Error*

The effect of the temporal truncation error on the eigenvalue deduced is examined. Expanding $F(t + 2\Delta t)$ in a Taylor series and using the DS scheme, the truncation error can be found to be $\bigcirc(\Delta t^3)$ from Section 4(b). Thus, for exponentially growing solutions, the numerical error in the amplification rate can be shown to be $\bigcirc(c_i^2\,\Delta t^2)$.

For $\Delta t \sim 0.4$, $c_i \sim 0.1$, truncation in time gives an error of about 0.15% in the eigenvalue irrespective of any additional error produced by spatial truncation and arithmetic inaccuracies.

(b) *Spatial Truncation Error*

A guide to the effect of the truncation error in height can be obtained by taking a flow with no mean wind, in which case $G \propto \cos n\pi z$. Neglecting the y-variation and putting the finite-difference replacement of G as G^*, then

$$\frac{\partial^2 G^*}{\partial z^2} = \frac{\partial^2 G}{\partial z^2} + \frac{(\Delta z)^2}{4!} \frac{\partial^4 G}{\partial z^4}.$$

With c^* the eigenvalue when using G^*, c the eigenvalue when using G, (6) becomes $-c(G_{zz} - \nu^2 G) + \gamma G = 0$, replaced by $-c^*(G^*_{zz} - \nu^2 G) + \gamma G = 0$, and then

$$\left| \frac{c - c^*}{c^*} \right| = \frac{(\Delta z)^2(\partial^4 G/\partial z^4)}{4!\,((\partial^2 G/\partial z^2) - \nu^2 G)} \sim \frac{(\Delta z)^2}{2.5} \qquad \text{for the 1st mode.}$$

With $\Delta z \sim \frac{1}{6}$, this implies an error of $\sim$1 % in the eigenvalue, which is considerably more than that due to the temporal truncation.

6. Iteration Error

At each time step it is necessary to solve a Laplacian equation and this was done by a relaxation technique. Iteration is terminated when the solution is within a given error of the analytic solutions to the set. Let this error be ϵF (small $|\epsilon|$) and consider the error it will produce in the eigenvalue.

The maximum error is given by

$$E_c = \frac{1}{2\Delta t} \log \left| \frac{(1+\epsilon)}{(1-\epsilon)} \right| \sim \frac{|\epsilon|}{\Delta t}. \tag{11}$$

Therefore, for given E_c and $|\epsilon|$, $|\epsilon| < \Delta t\, E_c$, and we note that there is, surprisingly, a lower bound to the time step. This becomes obvious if we note that with a small time step, the iteration error may become of the same magnitude as the increment in the eigenfunction. Thus, those temporal integration schemes that demand a small time step correspondingly demand accurate spatial solution if their accuracy is to be maintained.

This lower bound for the time step gives a guide to the maximum allowable iteration error. Returning to dimensional parameters,

$$|\epsilon| < \lambda \alpha_1 H\, \Delta T\, E_c$$

and Δt is taken as 1000 sec. Then, with $\alpha_1 H \sim 20$ msec^{-1} and $\lambda = 2 \times 10^{-6}$ m^{-1} (for a wavelength of $\sim$3000 km)

$$|\epsilon| < 4.10^{-2} E_c,$$

and for a 5 % error in c_i, $|\epsilon| < 0.002$.

Referring back to the various methods of time integration discussed in Section 4, the condition that the solution of the finite replacement to (8) must be found accurate to $E_c\,\Delta t$ of its analytic (or true) value has the following implications. For the forward time integration scheme of Section 4(a), with $E_c \sim (\Delta t/2)$ and $\Delta t \sim 0.02$; $E_c\,\Delta t \sim 2.10^{-4}$. This accuracy is quite unrealistic for the scheme to be of practical use while the DS scheme of Section 4(c) requires an accuracy of $\sim 2.10^{-3}$, which is of reasonable proportions.

7. The Vertical Resolution

We now examine the consequences of increasing the resolution and show that the tolerance to which the solution must be obtained is proportional to the square of the vertical grid length. The finite-difference equations solved at each time step can be written as

$$\mathscr{L}F_{k,l} \equiv \frac{1}{\Delta z^2}(F_{k,l+1} + F_{k,l-1}) + \frac{N}{\Delta y^2}(F_{k+1,l} + F_{k-1,l}) - \left(\frac{2N}{\Delta y^2} + \frac{2}{\Delta z^2} + \nu^2\right) F_{k,l} = G_{k,l} \tag{12}$$

where $F_{k,l}$ is the value of F at the point (k, l), $G_{k,l}$ is a known combination of $F_{k,l}$ at the previous time step, and $(2N/\Delta y^2) + (2/\Delta z^2) - \nu^2 = D$.

Typical values of N vary between 0.04 and 1 (for channel widths of 10,000–2,000 km) and ν between 0.5 and 2.5 (for wavelengths of 12,000 km–2,500 km). Thus, for small values of Δz (e.g., $<1/15$, and taking $\Delta y \sim \Delta z$), D is determined to within less than 1% by the value of ν. Therefore, unless (12) is solved to a high degree of accuracy at each time step, it will not be possible to distinguish changes in solution for small changes in ν, and to obtain a meaningful spectrum, growth rates and phase speeds must be found accurately enough to detect their changes for changes in wavenumber ~ 0.05.

8. Iterative Solution, Tolerance

A criterion for the termination of the iterative solution is examined in terms of the vertical resolution (Δz) using analysis based on [12] where the set (12) is solved at each time step by successive overrelaxation (e.g., [13]).

Let the ith iteration be $F_{k,l}^{(i)}$. Then the corresponding residual $R_{k,l}^{(i)}$ is given by

$$R_{k,l}^{(i)} = \mathscr{L}F_{k,l}^{(i)} - G_{k,l}$$

and the $(i+1)$th iteration is then

$$F_{k,l}^{(i+1)} = F_{k,l}^{(i)} + \alpha R_{k,l}^{(i)}/D \tag{13}$$

where α is the overrelaxation parameter.

Define $\eta_{k,l}^{(i)}$ as

$$1/\eta_{k,l}^{(i)} = | F_{k,l}^{(i+1)} - F_{k,l}^{(i)} |/| F_{k,l}^{(i)} |,$$

and $\epsilon_{k,l}^{(i)}$ as $\epsilon_{k,l}^{(i)} = (F_{k,l}^{(i)} - F_{k,l}^{an})$, the deviation of the ith iterate from the analytic solution.

Then $\epsilon_{k,l}^{(i)} = R_{k,l}^{(i)}$ and by expanding $\epsilon_{k,l}^{(i)}$ in a double Fourier series, it can be shown (as in [12]) that

$$(\pi^2(1 + N) + \nu^2) | \epsilon_{k,l}^{(i)} | < | R_{k,l}^{(i)} |. \tag{14}$$

Then if

$$1/\eta_{k,l}^{(i)} < \alpha | \epsilon_{k,l}^{(i)} | (\pi^2(1 + N) + \nu^2)/DF_{k,l}^{(i)}, \tag{15}$$

the iteration has converged to within $| \epsilon_{k,l}^{(i)} |$ of the analytic solution. Eq. (19) implies that the residuals in (17) are all small enough for convergence. From Section 6, (with $\epsilon = \epsilon^{(i)}/F^{(i)}$), $| \epsilon | < E_c \Delta t$ for convergence and with $\nu \sim 2$, $D \sim 2/\Delta z^2$, and $\alpha \sim 1$, (19) implies

$$1/\eta_{k,l}^{(i)} < \sim(1/2)(4 + \pi^2) E_c \Delta t \Delta z^2$$

and if at all gridpoints $\eta_{k,l}^{(i)}$ is less than η where

$$1/\eta = \sim(1/2)(4 + \pi^2) E_c \Delta t \Delta z^2, \tag{16}$$

the iterative has converged sufficiently. The parameter η is defined as the tolerance. Thus, for given $E_c \Delta t$ (determined from 4c, i.e., $E_c \sim \Delta t^5/4$), the tolerance criterion is

$$1/\eta \sim (\Delta z)^2. \tag{17}$$

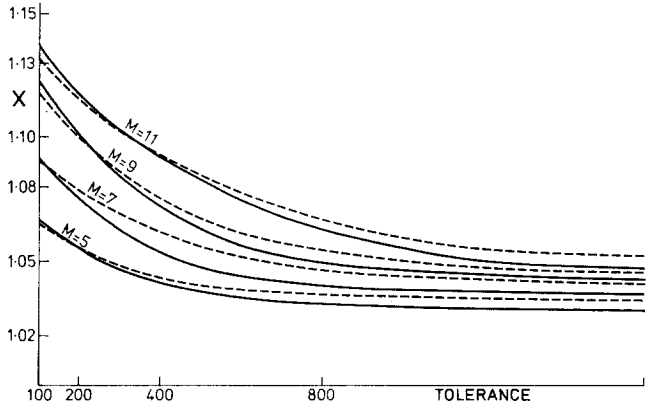

FIG. 3. Streamfunction at lower boundary mid-latitude (X) against tolerance for $U = z \exp(-2y^2)$, $L = 10{,}000$ km, $\gamma = 1$ with number of levels (M). Continuous curves for wavenumber 1.6; dashed curves for wavenumber 1.65.

Figure 3 illustrates the convergence of the iteration with differing numbers of levels.

We see from Fig. 3 that the effect of increasing the vertical resolution is an increase in the tolerance for convergence, as proposed by (16). If the iteration is stopped prematurely, the solution obtained will correspond to the solution at a different wavenumber and the eigenvalue spectrum will be distorted. Thus, with 11 levels (i.e., 9 layers between surface and tropopause), termination of the iteration at $\eta = 1000$ can be interpreted as a wavenumber error of ~ 0.05, which is a substantial error in the context of numerical prediction and in the spectrum drawn in Fig. 1.

9. Overrelaxation Parameter

Figures 4–6 illustrate the behavior of the parameter α in (13) for the flows of Fig. 3 for 5, 7, and 9 levels, respectively. A value of 1.3 for α appears to be the optimum and this was used in the following calculations.

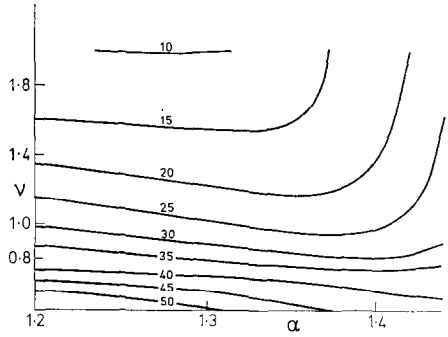

Fig. 4. Iterations against over-relaxation factor (α) and wavenumber (ν), five levels, $U = z\exp(-2y^2)$, $L = 10{,}000$ km.

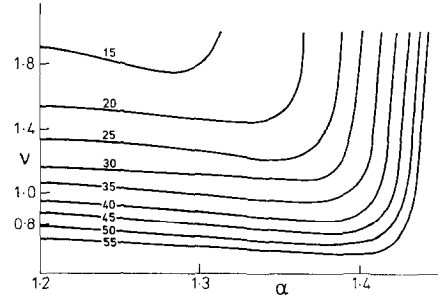

Fig. 5. As for Fig. 4, with seven levels.

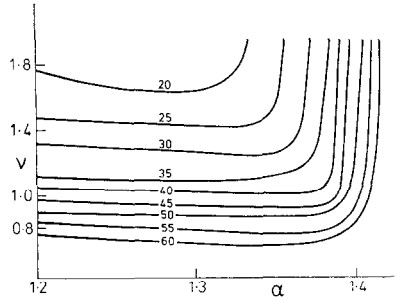

FIG. 6. As for Fig. 4, with nine levels.

10. ITERATIONS AGAINST TOLERANCE. OPTIMUM RESOLUTION

Figure 7 shows the variation of tolerance against number of iterations for the flow of Fig. 3 for 5, 7, 9, and 11 levels. For fewer levels, there is a large increase in tolerance for only a small increase in the number of iterations. As the number of levels increases, this becomes less marked.

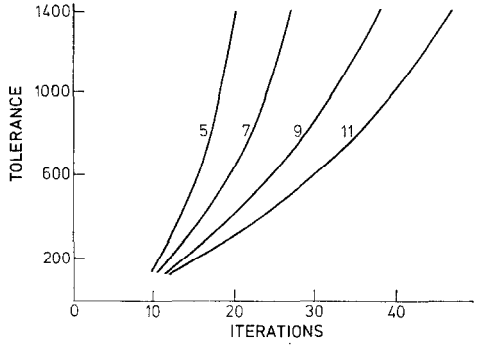

FIG. 7. Number of iterations against tolerance for 5, 7, 9, and 11 levels. $U = z\exp(-2y^2)$, $L = 10{,}000$ km.

By combining the results of Figs. 3 and 7 and using $5 \times 10^{-4}mn$ sec as the computer time needed for one iteration on the $m \times n$ grid, an optimum number of levels is obtained (there are $m - 1$ levels). Assuming convergence of the time integration to be about 400 repetitions of solving (12) (about 250 time steps) and allowing 500 sec of time to evaluate one eigenvalue and using $n = 10$, $mI \sim 250$ (I is number of iterations).

For $m = 10$, $\eta \sim 1{,}500$ (from Fig. 3) and then $I \sim 40$ (from Fig. 7), giving $mI = 400$, while for $m = 8$, $\eta \sim 900$ with I then ~ 20 and $mI = 160$. Thus, $m = 9$ (eight levels) will apparently give an optimum for the above computing time restrictions. With $\Delta t = \frac{1}{3}$ and using $\eta = 1000$, (16) implies $E_c \sim \pm 0.005$, which is acceptable.

11. Iterations Against Wavenumber. Redefined Tolerance

Figure 8 illustrates the effect of wavenumber on the iterative process. There is an increase in number of iterations needed to obtain a desired tolerance as the

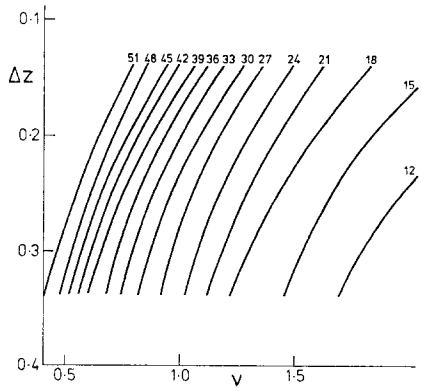

Fig. 8. Number of iterations against wavenumber (ν) and vertical gridlength (Δz) for tolerance 400.

wavenumber decreases. Thus, to obtain very long waves, the optimum of eight levels is considerably reduced.

12. Convergence from an Initial Eigenfunction Expansion

An initial guess of the stream function is made at all gridpoints and (12) is solved iteratively at each time step, the iteration being stopped when the appropriate tolerance is reached. At each time step, the growth rate at each gridpoint (except those with very small function values) is calculated and the time integration stopped when the growth rates differ by less than $\pm E_c$. Thus, the eigenfunction and related eigenvalue (with the largest imaginary part for the fastest growing wave) is found at each wavenumber.

With reference to Fig. 1, three problems are immediately apparent: (i) At certain wavenumbers, cusps occur where two waves grow at the same rate and there is no dominant wave. (ii) For very long and very short waves, the growth rates are small, so that the time taken for one solution to dominate over the others will be large, (iii) The above method will, in any case, only find the dominant wave, and other modes will be filtered out.

To alleviate these problems, consider the following approach: Integrate for $(2r - 1)$ time steps $(r = mn)$, each step being $2\Delta t$ using the DS method of Section 4(c), giving

$$F_\tau = F(y, z, 2\tau\,\Delta t), \qquad 0 \leqslant \tau < 2r \qquad \text{for wavenumber } \nu.$$

Then F_τ can be written as the sum of eigenfunctions (notice that there will be $m \times n$ of these, corresponding to the number of roots of the finite-difference characteristic equation) as:

$$F_\tau = \sum_{j=1}^{r} A_j \chi_j{}^\tau, \qquad \chi_j = e^{-2ic_j \Delta t} \tag{18}$$

and the $2r$ equations (18) can be solved for the $2r$ unknowns A_j, χ_j (with the same solutions at all gridpoints). A general method of solving (18) is based on an idea of Prony [14].

Consider the rth order difference equations $(0 \leqslant \tau - r < r)$

$$G_r F_\tau + G_{r-1} F_{\tau-1} + \cdots + G_1 F_{\tau-(r-1)} + F_{\tau-r} = 0 \tag{19}$$

with solution

$$F_\tau = \sum_{j=1}^{r} q_j \chi_j{}^\tau, \qquad \text{where} \qquad G_r \chi_j{}^r + G_{r-1} \chi_j{}^{r-1} + \cdots + 1 = 0. \tag{20}$$

But (20) is identical to (18) and hence χ_j are the roots of (20). Therefore, solve (19) for the G_r, then solve (20) for the χ_j, and finally, solve (18) for the A_j.

In practice the above method necessitates the solution of a high-order polynomial equation at each gridpoint and a variation of the method is considered.

As the integration proceeds, F_τ will be dominated by these eigenfunctions with large growth-rate and we may assume that, after a certain time, only three modes remain. Now r can be taken as 3 and (20) will be cubic. If the integration is carried out in sets of six time steps and (18)–(20) are solved at each gridpoint, three waves can be found for each wavenumber and the problem of the coincident growth rate at the cusps can be eliminated.

By choosing the initial perturbation to be similar to that of a dominant mode, the convergence time of the integration may be speeded up considerably.

13. Two Tests

(a) The preceding ideas were tested on a grid with 10 horizontal points and 8 levels, using the flow used for Figs. 1 and 2 so that results could be compared. At all wavenumbers the initial perturbation was assumed to be of the form

$$F_{k,l} = 1 + i$$

with $\Delta t = \frac{1}{8}$, $\eta^* = 1{,}300$, and $E_c = \pm 0.005$. The following wavenumbers were used

$$\nu = 0.8, 1.2, 2.0$$

where, from Fig. 1, we can see that the fastest growing modes were the fifth, third, and first for the symmetric type and fourth, fourth, and second for the anti-symmetric type, respectively, for the above wavenumbers.

The average convergence time was 250 steps, with slower convergence at low wavenumbers. The growth rate and phase speed spectra are shown in Figs. 9 and 10.

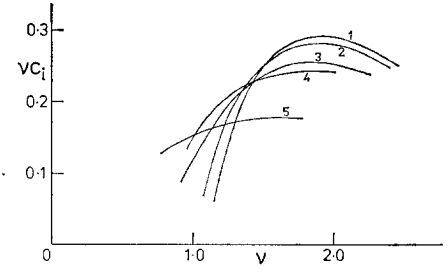

FIG. 9. Growth rate (νc_i) against wavenumber (ν) for $U = z$, first five modes by time integration.

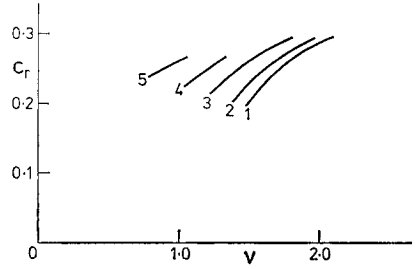

FIG. 10. Phase speed (c_r) against wavenumber (ν) for $U = z$, first five modes by time integration.

The eigenvalues of the nondominating modes (e.g. third and fifth at $\nu = 2.0$) were found by using approximate representations of these modes as initial perturbations, and the convergence time was thereby speeded up to about 120 steps, as suggested at the end of Section 12.

The correlation between Figs. 1 and 9 appears good, although no waves were obtained at wavenumbers less than the critical wavenumber at which waves do not grow (perhaps the growth rates were too small) and there was some doubt as to where the cusps actually occurred (although this would probably have been overcome if more wavenumbers were used in the vicinity of a suspected cusp).

(b) Although the power method was useful for the flow $U = z$, it may be less so for more realistic flows (say) of the form $U = z \exp -ky^2$, where growth rates of the dominant modes are very much greater than those of secondary modes because of the concentration of the sheared zone, and where, for similar reasons, at some wavenumbers the growth rate of even the dominant mode may be very small, thereby making convergence a long process.

A test was made on $U = ze^{-2y^2}$, with $\gamma = 1$ on the same grid as (a) and the eigenvalue spectra obtained are shown in Fig. 11. Convergence was rapid around $\nu = 1.8$ (about 100 time steps), but for long waves ($\nu \sim 1.2$) convergence was very slow (at least 300 steps). For the symmetric mode, another eigenvalue appeared

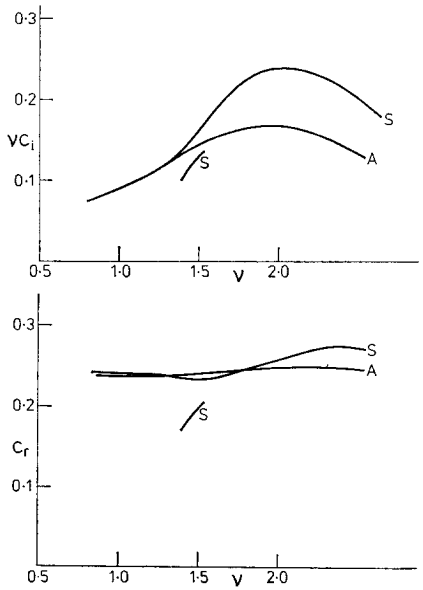

FIG. 11. Growth rate (νc_i) and phase speed (c_r) against wavenumber (ν) by time integration. $U = z\exp(-2y^2)$, $L = 10{,}000$ km, $\gamma = 1$. S is a symmetric mode; A is an antisymmetric mode.

at $\nu = 1.4$, but the method of trying to obtain this mode at another wavenumber but using it as an initial perturbation failed (probably due to its small growth).

Taking into account the above problems and the amount of computer time needed to obtain a reasonable spectrum (say, wavenumbers at intervals of 0.2 between 0.8 and 2.2) another method was sought for solving the eigenvalue problem. However, once the fastest growing wave is located the techniques described could be used on high resolution grids to examine the structure of the mode and its transfer properties.

14. Classical Formulation and Q.R. Algorithm

An alternative approach to solving the eigenvalue problem is to write down the finite-difference replacements to Eq. (6) and to solve the resulting algebraic set for c (the basic method used in [7] for the one-dimensional problem, though it was found convenient to use analytic methods for very long and very short wavelengths).

With $\mathscr{L}$ as $(\partial^2/\partial z^2 + N(\partial^2/\partial y^2) - \nu^2)$ and $\mathscr{M}$ as $\mathscr{L}Az + (\gamma - NzA_{yy})$, (4) and (5) reduce to $\mathscr{L}c\psi = \mathscr{M}\psi$ which, upon left-hand multiplication by $\mathscr{L}^{-1}$, reduces to $\mathscr{N}\psi = c\psi$ where $\mathscr{N} = \mathscr{L}^{-1}\mathscr{M}$. This is now in the form of a classical eigenvalue problem, and an efficient method of solution is to use the Q.R. algorithm, [5, 15]. (Note that the Q.R. method factorizes the matrix into the product of a unitary and upper triangular matrix. Repeated factorizations result, in the infinite limit, in a matrix, the diagonal elements of which are the eigenvalues of the original matrix.)

For the matrix $\mathscr{N}$ (which is real), the eigenvalues are found by the Q.R. method using an IBM library routine and the corresponding eigenfunctions are found from the set of simultaneous equations using another IBM routine. The streamfunction is normalized to $+1$ at midchannel.

The matrix $\mathscr{N}$ (which is of order $m \times n$: the total number of gridpoints) must be read into the computer explicitly, and thus, for reasons of storage, there is a limitation on the size of grid. For the grid used in the tests of Section 13 there were 90 points for the symmetric mode and 81 for the antisymmetric mode. These numbers were of manageable proportion for the CDC 6400.

15. A Test Using the Q.R. Algorithm

The method was tested on the flow of Section 13(b) and the spectra obtained are shown in Fig. 12. The eigenvalues were obtained for all the modes and are exact in the sense that the only approximation arises from the truncation error. Only the two fastest growing modes are drawn for both the symmetric and antisymmetric case.

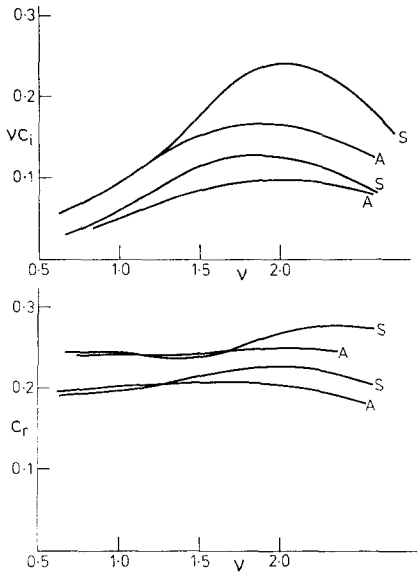

FIG. 12. Growth rate (vc_i) and phase speed (c_r) against wavenumber (v) by Q.R. algorithm. $U = z\exp(-2y^2)$, $L = 10{,}000$ km, $\gamma = 1$. S is a symmetric mode; A is an antisymmetric mode.

There is general agreement between Figs. 11 and 12 confirming the validity of the power method. There is a small difference between the corresponding growth rates of the secondary symmetric mode, probably due to an increased error in the time integration, and the failure to obtain this wave at wavenumbers other than $v \sim 1.5$ (due to its small growth rate) is confirmed. The computer time required to obtain the symmetric mode spectrum was 1500 sec, and this was a great saving compared to the power method solutions.

16. CONCLUSION

The Q.R. approach has the great advantage of speed and precision, but is somewhat limited by storage problems. However, for the purpose of investigating the structure of perturbation solutions, useful sized grids can be accommodated.

For treatment of finite amplitude waves this method is not available and some form of integration which is similar to the power method for small amplitudes must be used. Although the power series method of solving the potential vorticity equation is time consuming, it is possible to obtain solutions on high-resolution grids, taking into account the various convergence criteria and errors that appear and should not be discarded out-of-hand. (Recently, fast Fourier transform direct

methods have been analyzed and may alleviate some aspects of the spatial truncation that appear in the power method used in this paper.)

The results may be summarized as follows. First, although it is advantageous to have as great a resolution as possible, there is an inherent limit to which we may go. Apart from the increased number of points required for increased resolution, the tolerance to which a solution must be obtained is proportional to the square of the vertical gridlength and so are the number of iterations required to reach this tolerance. For practical purposes there is some suggestion of an optimum of about eight levels.

Second, it was found that there is a type of uncertainty principle connecting the time step, error in wave speed, and error in eigenfunction, and that the error in the eigenfunction is bounded by the product of the time step and error in the wave speed.

Examining the truncation error, it was found that a 1 % error in complex phase speed was possible, but that this accuracy could only be achieved if the finite difference problem was solved analytically, and an error larger than 1 % must b expected for iterative solutions.

A weakly unstable finite-difference scheme could be used for finding growing waves, and problems of degeneracy of solution could be eased by using a method whereby the time integration was terminated before all but one growing wave remained.

The final result, and perhaps the most important, was that for a reasonably accurate complete spectrum to be obtained, the time integration methods were too clumsy and time consuming while the direct Q.R. method of solution was both efficient and accurate. The disadvantage here was one of computer storage for a large grid, but once the wavelength of the most dominant wave was found, the time integration method could be returned to for examination of the wave structure at high resolutions.

ACKNOWLEDGMENTS

I would like to thank Dr. J. S. A. Green and other members of the Department of Meteorology at Imperial College for their help in the preparation of this paper.

REFERENCES

1. J. A. BROWN, JR., *J. Atmos. Sci.* **26** (1969), 352–366.
2. J. G. CHARNEY, *J. Meteor.* **4** (1947), 135–162.
3. E. T. EADY, *Tellus* **1** (1949), 33–52.

4. E. T. EADY, *Cent. Proc. R. Met. Soc.* (1950), 156–172.
5. J. G. F. FRANCIS, *Computer J.* **4** (1961, 1962), 265–271, 332–345.
6. FADE'EV AND FADE'EVA, "Computational Methods in Linear Algebra," (R. C. Williams, Trans.) Freeman, 1963).
7. J. S. A. GREEN, *Quart. J. R. Met. Soc.* **86** (1960), 237–251.
8. J. S. A. GREEN, *Quart. J. R. Met. Soc.* **96** (1963), 157–185.
9. E. N. LORENZ, *Tellus* **7** (1955), 397–407.
10. E. N. LORENZ, "The Nature and Theory of the General Circulation," World Meteorological Organisation, (1967).
11. M. J. MILLER AND R. P. PEARCE, *Quart. J. R. Met. Soc.* **100** (1974), 133–154.
12. K. MIYAKODA, *J. Met. Soc. Japan*, **38** (1960), 107–124.
13. G. D. SMITH, "Numerical Solution to Partial Differential Equations," O.U.P. (1965).
14. WHITTAKER AND ROBINSON, "The Calculus of Observations," Blackie, 1932.
15. J. H. WILKINSON, "The Algebraic Eigenvalue Problem," Clarendon Press, 1965.